NASA

Technical Memorandum 80718

(NASA-TM-80718) RADIO JUPITER AFTER VOYAGER: AN OVERVIEW OF THE PLANETARY RADIO ASTRONOMY OBSERVATIONS (NASA) 40 p
HC A03/MF A01 CSCL 03A

N81-20988

Unclas
G3/89 31317

Radio Jupiter After Voyager: An Overview of the Planetary Radio Astronomy Observations

A. Boischot , A. Lecacheux, M. L. Kaiser, M. D. Desch, J. K. Alexander and J. W. Warwick

JUNE 1980

National Aeronautics and Space Administration

Goddard Space Flight Center
Greenbelt, Maryland 20771

RADIO JUPITER AFTER VOYAGER: AN OVERVIEW OF THE PLANETARY RADIO ASTRONOMY OBSERVATIONS

A. Boischot
A. Lecacheux
Observatoire de Paris
Meudon, France

M. L. Kaiser
M. D. Desch
J. K. Alexander
Laboratory for Extraterrestrial Physics
Planetary Magnetospheres Branch
NASA/Goddard Space Flight Center
Greenbelt, Maryland 20771

J. W. Warwick
Radiophysics, Inc.
Boulder, CO 80301

SUBMITTED TO: Journal of Geophysical Research

Abstract

We present an overview of Jupiter's low-frequency radio emission morphology as observed by the Planetary Radio Astronomy (PRA) instrument onboard the Voyager spacecraft. The PRA measurement capabilities and limitations are summarized following over two years of experience with the instrument. As a direct consequence of the PRA spacecraft observations, unprecedented in terms of their sensitivity and frequency coverage, at least three previously-unrecognized emission components have been discovered: broadband and narrow-band kilometric emission and the lesser-arc decametric emission. Their properties are reviewed here. In addition, the fundamental structure of the decameter- and hectometerwavelength emission, which is now believed to be almost exclusively in the form of complex but repeating arc structures in the frequency-time domain, is described here for the first time. Dramatic changes in the emission morphology of some components as a function of sun-Jupiter-spacecraft angle (local time) are described. Finally, the PRA in situ measurements of the Io plasma torus hot-to-cold electron density and temperature ratios are summarized.

INTRODUCTION

The Voyager 1 and 2 (V1 and V2) Planetary Radio Astronomy (PRA) instruments detected radio bursts from Jupiter very shortly after launch and will likely continue to do so for at least another year. Thus, in a very real sense the PRA instruments are remote sensors capable of making observations of Jupiter from virtually any point in the solar system. Yet, the tremendous increase in Jovian signal strength relative to terrestrial or solar interference combined with the unique viewing geometry provided by the Voyagers make the encounter data sets one of the most important obtained in the 25-year history of the study of Jovian radio noise.

It is our intent in this paper to provide a brief review of the PRA findings that have already been published and an introduction to new results which appear in this issue. We will also address a number of PRA- and Jupiter-related topics which are important but which are either too brief to be deserving of separate consideration or which have otherwise not appeared in

previous PRA publications. We will begin by describing very simply the operation of the instrumentation including a discussion of the actual in-flight performance. We will then review the observations beginning with the decameter (DAM) wavelength measurements. We will compare the DAM observations made by PRA with those made by ground-based instruments, and we will show several examples of the extraordinary arc structures which are evident in the frequency-time plane. Then, for purposes of completeness and continuity with previous work, we will describe the PRA observations made at hectometer (HOM) wavelengths even though we now believe this spectral region to be just the low-frequency terminus of the DAM arcs. The newly-discovered kilometer (KOM) wavelength emissions show that two distinct and widely separated source regions contribute to this low-frequency portion of the Jupiter spectrum. We describe these data and discuss the inferences that can be made concerning their source locations. Finally, we will review the in situ measurements of electrostatic waves which were carried out during the 15-hr excursion through the Io plasma torus by V1.

INSTRUMENTATION

A detailed description of the PRA instrumentation can be found in Lang and Peltzer (1977) and Warwick et al. (1978). Here we summarize the radiometer characteristics as they relate to the interpretation of the PRA encounter data.

Both Voyager spacecraft carry identical radiometers consisting of two orthogonal 10-meter monopoles coupled to a single receiver. At low frequencies ($\lesssim$ 3 MHz) the antenna is substantially shorter than one wavelength and so, in principle, has the small radiation resistance and isotropic reception pattern of a Hertzian dipole. At higher frequencies the pattern undoubtedly becomes multilobed as the antenna elements begin to support more complicated current distributions. In practice, this idealized behavior is altered somewhat by the presence of the large conducting surfaces near the monopoles, such as the 13-meter magnetometer boom and the 3.7-meter diameter high-gain telemetry antenna. These bodies act as resonant parasitic elements for some antenna-source geometries. As might be expected, the low-frequency observations appear to have been affected the least, although we attribute the

problem V1 had in determining polarization sense at low frequencies before encounter (see Desch and Kaiser, 1980) to the presence of these structures. At higher frequencies, complete reversals in the polarization sense from one frequency band to another sometimes appear which are clearly instrumental in origin. The bands of frequencies most often affected are ∿ 5 MHz and ∿ 15 MHz on both spacecraft where the effective length of the monopoles are odd integral multiples of the wavelength. We have had to exercise caution in separating instrumental polarization reversals from the true reversals which are evident near these frequencies.

The PRA receiver functions as a stepped-frequency polarimeter in two broad frequency bands whose channel bandwidths and separations are different. The 1.2 - 1320 kHz low-frequency (LF) band consists of seventy 1.0-kHz wide channels, each separated by 19.2 kHz. The 1.2 MHz - 40.5 MHz high-frequency (HF) band consists of 128 channels, each of 200 kHz bandwidth. The separation between channels in the HF band is 307.2 kHz. The receiver ordinarily steps through the entire range from 1.2 kHz to 40.5 MHz in 6 sec, requiring 30 msec per channel increment. In this mode, the signal in each channel is averaged for 25 msec before digitization. The normal PRA data display mode is in the form of frequency-time dynamic spectra in which eight successive 6-sec scans are averaged together at each frequency. Higher data rate modes exist but results from these observations are preliminary and are not reported here.

The receiver dynamic range expressed logarithmically is 50 dB, and by inserting attenuators in the receiver preamplifiers in anticipation of particularly intense signals, a total effective dynamic range of 140 dB can be achieved. During the V1 and V2 encounters, ghost images of strong ∿6-MHz signals appeared on some dynamic spectra at 35 MHz and above. These ghost images are for the most part easily identifiable by virtue of their mirror image near 6 MHz and are not confused with actual high-frequency DAM.

Although the HF band should in principle be $(200/1)^{1/2} = 14$ times more sensitive than the LF band in detecting a signal against a uniform background, an extremely high level of noise in the HF band related to the high-speed switching logic in various spacecraft electronic systems greatly reduced its effective sensitivity. For this reason, the HF band observations of DAM were

limited to the period around Jupiter encounter as noted later. The excellent spacecraft noise rejection design employed in the LF band, on the other hand, enabled detection of Jupiter emission near 1 MHz almost immediately after launch. At V1 closest approach, detection threshold in the PRA LF band was 2×10^{-26} W m^{-2} Hz^{-1}. At 10 MHz in the HF band, where spacecraft noise was greatest, the minimum detectable flux was approximately 3×10^{-23} W m^{-2} Hz^{-1}. Toward the high-frequency end of the HF band, however, the detection thresholds are comparable to those found in the LF band. Finally, despite the fact that both V1 and V2 receivers were exposed for a considerable length of time to the intense radiation levels of Jupiter's magnetosphere and are approaching their projected 4-yr design lifetimes, no permanent failures have developed and both receivers are performing to specification.

The PRA radiometer determines polarization basically through the use of two orthogonal 10-meter monopoles independently coupled to a single receiver through a 90°-quadrature hybrid and a switch. As such, the system measures the left-hand (LH) and right-hand (RH) circularly polarized components of a wave, not its linear components or the phase difference between the components. This is equivalent to measuring only two of the four Stokes parameters necessary to completely specify the wave polarization state. Thus only the polarization sense of the wave, either LH or RH depending on which signal is stronger, can be determined unambiguously from a single measurement.

In spite of its limitations, this determination alone is invaluable in helping to specify source locations and emission modes and in distinguishing one emission source from another. Comparison of our polarization sense observations with ground-based measurements for the high-frequency ($\gtrsim$ 10 MHz) sources has shown that the PRA sense measurements are quite reliable. At lower frequencies, the polarization sense of previously undiscovered sources has been specified for the first time.

Under certain circumstances, it is also possible to make more specific quantitative estimates of the wave axial ratio (the ratio of the wave electric field minor-to-major axis). The indicated axial ratio as measured by the PRA instrument is a complex function of the degree of polarization of the wave, the wave tilt angle and the angle between the source direction and the normal

to the plane of our antennas. From a statistical sample of indicated axial ratio measurements and knowledge of the source direction, we can set bounds on both the true axial ratio and the degree of polarization.

OBSERVATIONS

We have separated the Jovian radio observations into four categories and two of these categories have each been further divided into two subcategories. Figure 1 delineates these categories and shows were they lie in frequency space relative to the PRA receiver channels. The highest frequency observations, in the DAM range, show "arc" structures when displayed in the frequency versus time plane. These arc structures divide into lesser and greater arcs depending on their spectral characteristics. We have called the extension of the arcs into the PRA low band HOM emission, although we do not believe this is a separate radio component. However, the KOM range consists of two clearly distinct components likely arising from widely separated source locations. Finally, during the 15-hour period centered on V1 closest approach, the PRA instrument became, in effect, a plasma wave receiver, and electrostatic waves associated with the Io plasma torus (IPT) were recorded.

We provide here an overview of the PRA findings and refer the reader to more detailed papers where applicable.

DAM. This description of the DAM observations is complementary to the detailed statistical study presented by Alexander et al. (this issue), and also utilizes the findings of Leblanc and Daigne (this issue) on arc morphology.

Many spectral characteristics of the DAM emission are known from ground-based observations (see for example, Carr and Desch, 1976) and can be summarized as follows:

The emission at frequencies above 20 MHz is very sporadic, with an occurrence probability dependent upon the System III Central Meridian Longitude (CML, see Seidelman and Devine, 1976) and Io phase coordinates of the observer, where Io phase is the departure of Io from superior conjunction

as seen by the observer. In particular the high frequency limit of the emission varies considerably but never exceeds 39.5 MHz. Below 10 MHz there are very few spectral observations, but the histograms of occurrence probability reveal strong changes in the emission characteristics. In particular the dependence on CML and on Io phase is different than at higher frequencies. The shape of the DAM spectrum is very repetitive for the same observer position in CML and Io phase, even for observations one Jovian year (12 years) apart (Alexander, 1974). The spectra show many kinds of fine structures. Some of them have been studied in detail: the modulation lanes (Riihimaa, 1976), the interplanetary scintillations (Douglas and Smith, 1967) and the ionospheric scintillations. The modulation lanes and interplanetary scintillations have characteristic times as short as a few seconds. Ionospheric scintillations and burst groups (Douglas, 1964) have time scales of minutes.

The Voyager measurements have produced several quite new results, mainly due to the fact that the observed frequency range extends down to below 1 MHz, and because, when the spacecraft are close to the planet, aside from the vastly improved signal strength, the emission is not perturbed by interplanetary scintillations or terrestrial ionospheric propagation effects. The most striking characteristic of the DAM spectra is that emission appears in nested families of arcs (Warwick et al., 1979a) in the frequency-time plane. This is very clear in Figure 2a. Often several families of arcs can be observed simultaneously, in particular at frequencies lower than 20 MHz. This contributes to the greater complexity of the occurrence probability and polarization histograms compiled from ground-based observations at frequencies below 20 MHz as compared to higher frequencies.

The arcs can be characterized by the frequency of their vertex (or "nose"), the sense of curvature of the arcs (vertex early and vertex late), their total extent in frequency ("lesser" arcs and "greater" arcs) and their curvature. Several families of arcs, possible corresponding to different sources of emission, can be recognized. This is studied in another paper [Leblanc and Daigne, this issue]. We note here some general characteristics of the arcs.

- For a given longitude, two kinds of arcs are generally observed (often simultaneously): one is limited to frequencies lower than 20 MHz (lesser arcs) and the other can reach much higher frequencies, 30 to 40 MHz (greater arcs).

- At a given frequency the average duration is of the order of 3 to 6 min, slightly larger for lesser than for greater arcs. This corresponds to a 2 to 4 degree rotation of the planet.

- The arcs are not periodic in time, but the delay between two consecutive arcs has an average value of 3 to 6 min, similar to the arc duration. This value is also slightly larger for the lesser arcs.

- The depth of the modulation by the arc structure, measured on fixed frequency plots like that in Figure 2b is variable but often larger than 20 dB.

- The emission along an arc is generally relatively smooth without variations faster than the six-second resolution of the PRA receiver.

- It is probable that all the arcs close at very low frequencies, i.e., df/dt becomes small when $f \to 1.3$ MHz, and some of them can be followed at frequencies below 1.3 MHz into the PRA low band. The lesser arcs often are also asymptotic (i.e., df/dt approaches zero) at an upper frequency between 10 and 20 MHz. On the other hand for greater arcs $df/dt \neq 0$ at their upper frequency limit, as if this limit were set by a phenomenon whose origin is different from that of the arcs themselves.

- Great arcs are nearly always RH polarized at frequencies $\geq$ 20 MHz. Lesser arcs exhibit a distinctive bimodal polarization pattern as a function of CML. They are generally LH polarized below 120° CML and are RH polarized between 140° and 300°. These trends directly confirm earlier ground-based polarization determinations (e.g., see the work of Kennedy, 1969).

- The relative intensity of the arcs of some of the different families changes between the pre- and post-encounter periods but this is not accompanied by a change in the arc shape.

The different traditional "sources" identified from the ground-based observations (see Carr and Desch, 1976) have very different characteristics from one another in the PRA data, and, within one source, are strongly dependent on the phase of Io and the CML. We shall only describe below the "typical" spectrum for each of the sources and give some examples.

Some examples of Source A or main source (190° < CML < 290°) are given in Figure 3g-3ℓ. The arcs are great, vertex late arcs, generally asymmetric around their vertex. This vertex lies around 10 to 12 MHz for the Io-controlled source. For a given CML, there is a change in arc shape correlated with the phase of Io. This change exists not only when comparing the so-called Io-controlled events (Figure 3j) with non-Io-controlled events (Figure 3i), but even at different Io phase values within the same non-Io-controlled "source" (e.g., Figure 3h vs. Figure 3i). The control exhibited by Io on the arc shape is certainly different than Io control of occurrence probability (Leblanc and Daigne, this issue). In particular, for Io phase in the range 100° to 200° we observe closely spaced arcs with small curvature, which can extend up to 30 MHz (Figure 3i).

Some examples of Source B or early source (60° < CML < 190°) are given on Figure 3a-3f. The arcs are great, vertex early arcs, often with an irregular high frequency limit. The curvature is small and the vertex frequency is around 20 MHz. The high frequency limit depends sensitively upon the exact position of Io during the emission. The non-Io-B source does not appear very different from Io-B, except by its intensity which is much less on the average and by the absence of a distinct band of emission of the kind that often bounds the upper frequency envelope of the Io-B spectrum.

Source Io-C or late source (290° < CML < 30°; 220° < phase of Io < 260°) corresponds to a few vertex late great arcs with a sharp upper frequency limit. The arc structure is not as well defined as for the other sources. Sometimes below 22 MHz those great arcs are superposed on a very irregular source of arcs modulated in intensity with frequency. The shape of this source is very dependent on the position of Io. An example of Io-C is shown in Figure 3i.

Source Io-D or fourth source always appears at early longitudes when the range of Io phase is between 90^{o} and 120^{o}. It corresponds to only one narrow band of emission extending very slowly to an upper frequency between 17 and 22 MHz as shown in Figures 3d.

The remarkable influence of the location of Io on the detailed appearance of dynamic spectra of the Io-related DAM is illustrated in Figure 4. Here we show a compilation of spectra for each of the four "sources" described above. All of the spectra in a particular column are aligned in CML, and they are ordered according to the time at which the Io phase reached the value associated with the statistical "center" (i.e., point of maximum occurrence probability) of the source as defined in plots of occurrence probability on the CML-Io phase plane. This special value of Io phase occurs before the CML of maximum occurrence probability for the top panel of each column in Figure 4 and after the CML of the occurrence probability peak for the bottom panel of the same column. A similar view of the effects of Io location on dynamic spectral features was presented by Dulk (1965) based on ground-based observations, and the new Voyager data complement and extend those findings.

Notice in Figure 4 that some major emission features tend to "follow" Io. When Io reaches a given phase angle at larger Jovian longitudes, the feature also occurs at larger CML values, although the shift in feature CML is only about half the shift in Io longitude. For example, in the B source spectra (left column of Figure 4b), the most intense emission at the highest frequencies tends to occur later in time when Io reaches 90^{o} phase at later longitudes. A similar trend is evident for the distinctive, narrow band of emission that drifts from low to high frequencies in source D (right column of Figure 4b) and for the last group of vertex late great arcs that extend from 1.3 MHz up to > 30 MHz in most source A events (left column of Figure 4a).

A prototype of the PRA receiver has been operated at the Nancay Radio Astronomy Observatory throughout the Voyager encounter periods with a high gain (25 dB) right-hand circularly polarized antenna array. Due to the earth's ionospheric cut-off and to the presence of manmade interference, the observations are generally limited to a minimum frequency of 10 MHz at night and 20 MHz during the day. The arc structure is evident in ground spectra,

but because of the low-frequency limit of the observations only the upper legs of the arcs are observed. Figure 5 shows a spectrum of the Io-B source (compare with Figure 4b) taken in Nancay with a spectrograph using higher time and frequency resolution capability than PRA. The dominant features seen on ground spectra are broadband (vertical) structures which correspond to the L bursts [see Carr and Desch, 1976]. They are not observed on the Voyager spectra, taken close to Jupiter and this is a confirmation that those variations are due to interplanetary and/or terrestrial ionospheric scintillations. On the other hand, the burst groups often described from ground-based measurements are probably due in part to the observation of successive arcs at a given frequency.

We must remark that even with the several orders of magnitude increased sensitivity provided by the Voyagers no emission has been observed extending above 39.5 MHz, and the relative occurrence probability for emission observed at frequencies above $\sim$35 Mhz is not larger than with less sensitive instruments. This means that the HF limit of the emission is a real cut-off that is very sharp and that is not set by the sensitivity of the observations.

As the arc structures appear to be fundamental to a large fraction of Jupiter's emission morphology, several papers appearing in this issue (Staelin; Goldstein and Thieman; Warwick; Boischot and Aubier; Pearce) are devoted exclusively to deriving arc forming mechanisms. Staelin (this issue) also presents a general introduction to the type of mechanisms presently being considered.

Another important property of the DAM emissions identified from the Voyager measurements is a strong dependence on local time (or, more precisely, observer-Jupiter-sun angle). The PRA data show the same concentrations of great arc DAM activity at values of CML corresponding to the A and B sources as are seen from the earth. However, the statistical analysis of Alexander et al. (this issue) and the study of dynamic spectra by Leblanc and Daigne (this issue) show that the relative levels of activity of the Io-independent emissions reverse after Voyager closest approach. When observed from above the dayside hemisphere the A source dominates at frequencies $\geq$ 20 MHz, but as seen from above the nighttime hemisphere after encounter, the B source

dominates and the non-Io-A emissions are weak and rare above 20 MHz. Alexander et al. suggest that, in the context of certain source models, this effect could be due to diurnal variations in the properties of the ionosphere at the source.

HOM. The emission below 1.3 MHz, i.e., in the PRA low band, has been extensively studied by the two Voyagers. In this range the PRA experiment is practically free from interference and has very good sensitivity. Emission below 1.3 MHz was observed immediately after launch when the spacecraft were more than 4 AU from Jupiter. A study of the HOM occurrence statistics as observed during the preencounter cruise mode has already been published (Kaiser et al., 1979). It shows that the emission appears in two sources localized in CML near 120° and 240°, and is not controlled by Io. The dynamic spectra have different shapes for the two sources (Lecacheux et al., 1980) which change systematically with the sub-Voyager latitude (Alexander et al., 1979). These cruise observations refer only to the most intense emissions, and a much more detailed study can be made when the spacecraft are closer to Jupiter.

The PRA low band dynamic spectra of Figure 6 cover ten rotations of the planet. The HOM emission is indicated along with the two newly discovered kilometer wavelength components (bKOM and nKOM) which will be described in the next section. The HOM emission, contrary to the bKOM, avoids the central meridian longitude (CML) when the north dipole tip is tilted toward the spacecraft. At other longitudes, the intensity in the HOM band decreases with decreasing frequency as can be seen in the bottom panel of Figure 6. Sometimes, when the spacecraft is close to the planet the HOM emission can be observed down to the lowest frequency of the PRA receiver, but the low frequency cut off does not appear to be as sharp as for the kilometric emissions. Drifting features are observed in the HOM range, the drift being more often toward low frequencies for CML < 180° and toward high frequencies for CML > 180°. These drifting features are more easily studied on dynamic spectra with better time resolution than in Figure 6 and can be interpreted as the lower legs of arcs which have their vertexes in the DAM range. On the other hand, there may be structures other than the arcs at frequencies below 1.3 MHz. This was suggested by the cruise mode observations (Lecacheux et

al., 1980). When the spacecraft were far from the planet several clear structures repetitive in CML were observed. More studies are required to determine if those structures are different from the arc structure, or if as we now believe they are only superposed arc structures. In addition, an interpretation of the hectometric spectral structures observed during V1's path through the Io torus was attempted using a ray tracing method (Lecacheux, this issue). In the limit of our knowledge of the electron density distribution inside the Io torus, the observed HOM source could be situated in the southern hemisphere in a wide range of longitudes, the emission frequency being related to the local gyrofrequency.

The upper panel of Figure 6 shows the sense of polarization as a function of time and observing frequency coded such that LH is black, RH is white, and gray represents equal power in both channels (i.e., randomly or linearly polarized). In the HOM band, the polarization pattern is very repeatable with RH generally evident between CML $\simeq 0^{\circ}$ and 90°. The RH emission is flanked by LH emission centered at CML $\simeq 330^{\circ}$ and 100°. This LH emission was the most easily observed during the preencounter cruise period (Kaiser et al., 1979) presumably due to its slightly higher intensity relative to the RH emission. The HOM polarization pattern observed from the outbound trajectories of both spacecraft is not as clear as the inbound pattern. There are some ranges of CML where the polarization may even have reversed relative to that observed before encounter. However, if the HOM band represents at least in part the low-frequency extension of DAM arcs, then the relative changes after encounter in the amplitude of the non-Io controlled arcs mentioned in the previous section could easily account for the apparent polarization changes (Alexander et al., this issue).

KOM. At the low-frequency end of the PRA spectrum, two distinct new radio components have been discovered. As shown in Figure 6, we have designated them bKOM, and nKOM for broad- and narrow-band kilometer wavelength emission, respectively. The bKOM emission was detected when the spacecraft were approximately 2 AU from Jupiter, while the nKOM events were generally recognized only on records taken inside 1/2 AU from Jupiter. The properties of bKOM have been described in considerable detail by Warwick et al. (1979a,b), Scarf et al., (1979), Kurth et al., (1979), and Desch and Kaiser

(1980). Some of the nKOM properties were first described by Warwick et al. (1979b), but the recognition of nKOM as a separate and distinct radio component was presented by Kaiser and Desch (1980).

bKOM. The bKOM component, which is the more intense of the two, extends upwards from a frequency close to the lower limit of the PRA receiver (20 kHz). During each rotation of the planet, the high frequency limit first increases with time to reach a peak generally between a few hundreds of kHz and 1 MHz, and then decreases, giving a tapered aspect as can be seen in all four panels of Figure 7, as well as in Figure 6.

As observed during the portion of the Voyager trajectory before Jupiter encounter, the peak frequency is generally reached when the CML is around 200°, i.e., when the north magnetic pole is tilted toward the observer. The total duration lies between a few minutes to two or three hours depending on observing frequency, so it is sometimes observed during a 100° rotation of the planet. Other characteristics of the bKOM emission spectrum are:

- The low frequency limit is generally observed in the range between 10 and 100 kHz. In Figure 7b, for instance, the emission is hardly seen at 40 kHz and is completely absent at 20 kHz. Similar cut-offs can be observed in some cases up to 200 kHz but in other cases the emission extends down to 10 kHz or less (Scarf et al., 1979).

- The emission is highly variable in intensity. Very distinct fine structures are seen which are generally narrow band and which drift in frequency with time, either toward low or high frequencies. These time structures can be seen on Figure 7a, b, and c. These drifting features are reminiscent of the arcs which are often seen at higher frequencies, but the relation between the two phenomena, if any, is not clear.

- The polarization sense, the average power, and even the appearance of bKOM on dynamic spectra is a strong function of the observer's local time. As viewed from before encounter, i.e., from above the Jovian dayside, the bKOM associated with CML = 200° is LH polarized with a dynamic spectral shape like that shown in Figure 6 and Figure 7a, b, and c. As viewed from after

encounter above the Jovian nightside, bKOM is RH polarized, the average power level is less by a factor of ten relative to dayside events, and the dynamic spectra often show a gap or "bite" with no emission detectable near CML = 200°, similar to the event shown in Figure 7d.

There appears to be a growing consensus as to the source location of bKOM. Green and Gurnett (1980) have had success in reproducing features of the overall bKOM spectral envelope by ray tracing the magnetoionic ordinary mode through the Io plasma torus from a source region which extends above Jupiter's northern auroral ionosphere. In substantial agreement, Desch and Kaiser (1980) further constrain this source to be fixed in local time in Jupiter's dayside in order to explain the dramatic post-encounter polarization and spectrum changes.

nKOM. The second type of emission observed at kilometric wavelengths, nKOM, has a much narrower spectrum, covering generally not more than 3 or 4 of the PRA channels, i.e., its total bandwidth is approximately 40 to 80 kHz. The events appear intermittently persisting for some minutes to several hours. During the period when it is observed, the emission has a nearly constant frequency. Most of the time, this frequency is around 100 kHz with very sharp low and high frequency cut-offs.

On fixed frequency records, the emission differs much from the bKOM emission. It is much smoother, with very litle fine structure, and varies slowly with time as can be seen on Figure 8. The polarization of nKOM shows no discernible variation with observer's local time. LH nKOM emission is detected when Voyager is above Jupiter's northern magnetic hemisphere and RH emission corresponds to the southern magnetic hemisphere.

Without question the most remarkable property of nKOM is the occurrence pattern as a function of CML. Figures 9a and b show the occurrence of bKOM (shaded) and nKOM (lines) versus CML for many rotations near the two encounters. The bKOM always occurs near the CML = 200° north dipole tip passage and, so, clearly recurs at the System III rotation rate. The infrequently observed component of bKOM associated with the south dipole tip is not shown. In contrast, the nKOM emission does not repeat at the same CML

rotation after rotation, but clearly slips by a small amount. During the V1 encounter period nKOM repeated at approximately 10^h 15^m intervals while during the V2 encounter at a 10^h 28^m repetition rate. This lack of strict adherence to the Jovian System III rotation period coupled with some qualitative ray tracing arguments have prompted Kaiser and Desch (1980) to suggest that the nKOM source region is in the Io plasma torus near the magnetic equatorial plane at 8-9 R_J from the center of Jupiter. This is in direct contrast to the other Jovian radio components, all of which recur at the System III rate and are thought to originate from low to moderate altitudes above the Jovian ionosphere.

Io Plasma Torus. Although the bulk of the PRA observations have been of freely-propagating electromagnetic radiation, the V1 approach to within a Jovicentric distance of 4.9 R_J afforded us direct in situ measurement of the upper hybrid resonance (UHR) and (n+1/2) gyroharmonic electrostatic waves associated with the dense Io plasma torus (IPT). Based on the observations of the UHR lines, Warwick et al., (1979a) were able to construct a plasma density contour map of the IPT whose 500 cm^{-3} contour extended from inside 5 R_J to nearly 8 R_J in the equatorial plane and over 1 R_J above and below the plane. Extrapolations suggested a maximum electron density in the plane of above 3500 cm^{-3} near 5.6 R_J. These measurements provided the first electron density model of the IPT.

Birmingham et al. (this issue) enlarge substantially upon the preliminary analysis of Warwick et al. They present a thorough description of the observed electrostatic wave morphology and results of a detailed application of plasma instability theory (Hubbard and Birmingham, 1978) to the wave observations. A portion of the observations to which this theory is applied is shown in Figure 12. Here, the UHR and gyroharmonic waves present during the outbound pass ($\sim$ 6 R_J to $\sim$ 9 R_J) through the IPT are plotted. Each trace is an intensity vs time plot at a particular frequency from 20 to 328 kHz. The smooth, wavelike enhancements, particularly noticable at 40 and 59 kHz, are (n + 1/2) gyroharmonic waves, whereas the bursty signatures (cf., 1800 SCET at 116 kHz) are identified as UHR emissions. Reference to the seven sloping lines, which locate the electron gyrofrequency f_g and its harmonics as derived from the measured magnetic field values (Ness et al., 1979), shows

that the UHR and (n+1/2) gyroharmonic emissions clearly occur between the gyrofrequency harmonics. Birmingham et al. use this information and the steadily evolving pattern of change in the location of the UHR line relative to the (n+1/2) gyroharmonic to estimate cold-to-hot temperature ratios (T_C/T_H) for a two-component electron plasma throughout the torus. They find that T_C/T_H varies smoothly from $\leq$ 0.01 to 0.04 in moving outward from about 5 to 8 R_J through the IPT. Birmingham et al. also revise the original contour model somewhat after reexamining the UHR morphology and assuming symmetry about the centrifugal instead of the magnetic equatorial plane. Thus far, all of the IPT temperature and density modeling derived from the PRA observations either complements or reinforces measurements by other Voyager investigators (e.g., Bagenal et al., 1980; Strobel and Davis, 1980; Scudder and Sittler, this issue).

SUMMARY

The study of the dynamic spectra of Jovian emissions observed by the PRA experiment allows us to recognize at least three kinds of emission, with certainly different origins.

The most striking characteristic DAM emission is that it always appears as nested discrete arcs. Several families of arcs are observed simultaneously. Their dynamic spectral shape, sense of curvature, and frequency extent are repeatable functions of CML and Io phase. The Io-related emissions generally reach greater intensities and higher frequencies while the Io-independent emissions tend to be weaker and more sporadic and to depend on observer's local time. Nevertheless, the basic similarities in all the emissions suggest that both the Io-related and the Io-independent sources share a common radiation mechanism and/or a common range of source locations.

The HOM emission has some characteristics different from those of DAM, but other characteristics are similar to those of the DAM emission, in particular the presence of arcs. There is no clear evidence that HOM is a phenomenon really distinct from DAM or that it represents a different physical mechanism, but more careful investigations of the Voyager spectra, particularly near the 1.3 MHz discontinuity of the receiver, are necessary to clear up this point.

The bKOM emission is a highly irregular, very intense emission, observed when the magnetic dipole tip is tilted toward the observer. The frequency range, polarization sense, and local time variations of bKOM suggest that the emission is generated in the dayside auroral zone. The characteristic tapered appearance may be caused by refraction in the Io plasma torus.

The nKOM emission, is certainly a phenomenon different from the bKOM. This is clear from the differences in their spectrum and from their different occurrence patterns in CML. The statistical analysis of their occurrence shows that the source likely originates in the outer part of the torus but the mechanism of the emission is not known yet.

The Io plasma torus has been modeled now in terms of its electron density and ratio of cold-to-hot electron temperatures. These measurements will have bearing on the general problem of Io's interaction with the Jovian magnetosphere and Io's internal structure.

ACKNOWLEDGMENT

Our colleagues A. C. Riddle, J. B. Pearce, T. D. Carr, S. Gulkis, Y. Leblanc, B. M. Pedersen, D. H. Staelin, R. G. Peltzer, F. T. Haddock, W. E. Brown, Jr., R. J. Phillips, J. J. Schauble, and J. R. Thieman participated in various phases of this investigation. Our experiment representative at JPL, R. L. Poynter, and our data analyst at GSFC, P. G. Harper provided invaluable assistance in the day-to-day operation of the experiment. Our French investigators acknowledge support by Centre National d'Etudes Spatiales. This work was also supported, in part, by JPL under NASA contract NAS7-100.

REFERENCES

Alexander, J. K., Note on the beaming of Jupiter's decameter-wave radiation and its effect on radio rotation period determinations, Astrophys. J., 195, 227, 1974.

Alexander, J. K., M. D. Desch, M. L. Kaiser, and J. R. Thieman, Latitudinal beaming of Jupiter's low frequency radio emission, J. Geophys. Res., 84, 5167, 1979.

Alexander, J. K., T. D. Carr, J. R. Thieman, J. J. Schauble and A. C. Riddle, Title to be decided later, J. Geophys. Res., this issue.

Bagenal, F., J. D. Sullivan, and G. L. Siscoe, Spatial distribution of plasma in the Io torus, Geophys. Res. Lett., 7, 41, 1980.

Birmingham, T. J., J. K. Alexander, M. D. Desch, R. F. Hubbard and B. M. Pedersen, Observations of electron gyroharmonic waves and the structure of the Io plasma torus, J. Geophys. Res., this issue.

Boischot, A., and M. Aubier, The Jovian decametric arcs as an interference pattern, J. Geophys. Res., this issue.

Carr, T. D. and M. D. Desch, Recent decametric and hectometric observations of Jupiter, Jupiter, edited by T. Gehrels, p. 693, University of Arizona Press, Tucson, 1976.

Desch, M. D. and M. L. Kaiser, The occurrence rate, polarization character, and intensity of broadband Jovian kilometric radiation, J. Geophys. Res., in press, 1980.

Douglas, J. N., Decametric radiation from Jupiter, IEEE Trans. Military Electronics, MIL-8, 173, 1964.

Douglas, J. N. and H. J. Smith, Interplanetary scintillation in Jovian

decametric radiation, Astrophys. J., 148, 885, 1967.

Dulk, G. A., Io-related radio emission from Jupiter, Ph.D. dissertation, University of Colorado, Boulder, CO, 1965.

Green, J. L., and D. A. Gurnett, Ray tracing of Jovian kilometric radiation, Geophys. Res. Lett., 7, 65, 1980.

Goldstein, M. L. and J. R. Thieman, On the formation of arcs in the dynamic spectra of Jovian decameter bursts, J. Geophys. Res., this issue.

Hubbard, R. F. and T. J. Birmingham, Electrostatic emissions between electron gyroharmonics in the outer magnetosphere, J. Geophys. Res., 83, 4837, 1978.

Kaiser, M. L., M. D. Desch, A. C. Riddle, A. Lecacheux, J. B. Pearce, J. K. Alexander, J. W. Warwick, and J. R. Thieman, Voyager spacecraft radio observations of Jupiter: initial cruise results, Geophys. Res. Lett., 6, 507, 1979.

Kaiser, M. L. and M. D. Desch, Narrow band Jovian kilometric emission: a new radio component, Geophys. Res. Lett., in press, 1980.

Kennedy, D. J., Polarization of the decameter radiation from Jupiter, Ph.D. dissertation, University of Florida, Gainesville, FL, 1969.

Kurth, W. S., D. A. Gurnett, and F. L. Scarf, Spatial and temporal studies of Jovian kilometric radiation, Geophys. Res. Lett., 7, 61, 1980.

Lang, G. J., and R. G. Peltzer, Planetary radio astronomy receiver, IEEE Trans., AES13, 466, 1977.

Leblanc, Y., and G. Daigne, On the arc structure of the DAM Jovian emission, J. Geophys. Res., this issue.

Lecacheux, A., Ray tracing in the Io plasma torus: application to the PRA observations during Voyager 1's cloest approach, J. Geophys. Res., this

issue.

Lecacheux, A., B. Pedersen, A. C. Riddle, J. B. Pearce, A. Boischot and J. W. Warwick, Some spectral characteristics of the hectometric Jovian emission, J. Geophys. Res., in press, 1980.

Ness, N. F., M. H. Acuna, R. P. Lepping, L. F. Burlaga, K. W. Behannon and F. M. Neubauer, Magnetic field studies at Jupiter by Voyager 1: preliminary results, Science, 204, 982, 1979.

Pearce, J. b., A heuristic model for the Jovian decametric arcs, J. Geophys. Res., this issue (maybe).

Riihimaa, J. J., Polarization patterns in the dynamic spectra of Jupiter's decametric radio bursts, Astron. Astrophys., 53, 121, 1976.

Scarf, F. L., D. A. Gurnett, and W. L. Kurth, Jupiter plasma wave observations: an initial Voyager 1 overview, Science, 204, 991, 1979.

Scudder, J. D. and E. C. Sittler, A survey of the plasma electron environment of Jupiter: direct measurements, J. Geophys. Res., this issue.

Seidelmann, P. K. and N. Divine, Evaluation of Jupiter longitudes in System III (1965), Geophys. Res. Lett., 4, 65, 1977.

Stroebel, D. F. and J. Davis, Properties of the Io plasma torus inferred from Voyager EUV data, Ap. J. Lett., in press, 1980.

Staelin, D. H., Models for the origin of Jovian decametric emission, J. Geophys. Res., this issue.

Warwick, J. W. Models for decametric arcs, J. Geophys. Res., this issue.

Warwick, J. W., J. B. Pearce, R. G. Peltzer, and A. C. Riddle, Planetary radio astronomy experiment for the Voyager missions, Space Sci. Rev., 21, 309, 1977.

Warwick, J. W., J. B. Pearce, A. C. Riddle, J. K. Alexander, M. D. Desch, M. L. Kaiser, J. R. Thieman, T. D. Carr, S. Gulkis, A. Boischot, C. C. Harvey, and B. M. Pedersen, Voyager 1 planetary radio astronomy observations near Jupiter, Science, 204, 955, 1979a.

Warwick, J. W., J. B. Pearce, A. C. Riddle, J. K. Alexander, M. D. Desch, M. L. Kaiser, J. R. Thieman, T. D. Carr, S. Gulkis, A. Boischot, Y. Leblanc, B. M. Pedersen, and D. H. Staelin, Planetary radio astronomy observations from Voyager 2 near Jupiter, Science, 206, 991, 1979b.

Figure Captions

Figure 1. The PRA frequency coverage and the relevant frequencies of the various components in Jupiter's spectrum.

Figure 2. a) A dynamic spectral display of over two hours of Jovian activity recorded on March 5, 1979 by Voyager 1. In this and subsequent figures, increasing received power is indicated by increasing darkness. The system III longitude and Io phase angle are shown at the top of the figure. The obvious change in spectral appearance at 1.3 MHz simply reflects the receiver bandwidth and channel spacing differences between the PRA low band and high band. The so-called lesser arcs are centered near 10 MHz and persist throughout the panel, wherease, the great arcs are seen only between 23 and 00 hr above 15 MHz. b) Single frequency cuts across panel a showing the intensity variations as a function of time.

Figure 3. A compilation of dynamic spectra from the PRA high frequency band shown as a function of System III longitude. The corresponding Io phase at the beginning of each panel is shown in the lower left corner of each panel. Io phase increases approximately 49° across a panel.

Figure 4. A compilation of dynamic spectra of Io-related DAM events arranged to shown the variation in spectral features as a function of Io phase. (a) A series of source A events (left column) and a series of source C events (right column). (b) A series of source B events (left column) and a series of source D events (right column). All panels are aligned in CML and the arrow at the top of each panel denotes the time at which the Io phase was at the value corresponding to maximum occurrence probability for the particular "source". The dates and spacecraft-Jupiter distance in Jupiter radii (R_J) are given for the mid-point of each Voyager-1 (V1) and Voyager-2 (V2) spectrum.

Figure 5. A dynamic spectrum recorded by ground-based equipment in Nancay, France on January 8, 1980. The spectrograph used has higher frequency and time resolution than the PRA receiver.

Figure 6. Polarization (top panel) and total power (bottom panel) dynamic spectrum showing typical examples of HOM, bKOM and nKOM emissions. The spectrum spans 9-1/2 rotations of the planet and covers the frequency range from 20 to 1320 kHz. The polarization sense convention is indicated to the right of the top panel. Note that the bKOM events are uniformly anticoincident with HOM and that both components are locked in System III longitude (topic marks). On the other hand, nKOM drifts in longitude. Solar type III bursts are apparent at ∿ 12 hr and 22 hr on May 29.

Figure 7. Dynamic spectra from the PRA low-frequency band showing the general appearance of bKOM. The top three panels, recorded during the pre-encounter legs, show the occurrence concentration near longitude 200°. The bottom panel, recorded after encounter, shows the often-observed "gap" in the emission at this same longitude. Narrow-band drifting features can also be seen, particularly in the top two panels.

Figure 8. Intensity versus time displays for several PRA low-frequency channels recorded on May 27, 1979 by Voyager 2. The bKOM emission centered at 01, 11, and 21 hr is bursty in appearnace and extends across the entire frequency range shown. The nKOM emission at 05 and 16 hr has a much smoother envelope and typically is observed on only three channels.

Figure 9. The occurrence as a function of CML of bKOM (shaded) and nKOM (lines) during the V1 encounter period (a) and V2 encounter period (b).

Figure 10. Intensity-time tracings of gyroharmonic lines in the IPT recorded at 17 discrete frequency channels. Within each trace, identified by its frequency in kHz, the vertical dimension is logarithmically proportional to intensity. The variation in time of the electron gyrofrequency and its first six integral harmonics is shown superposed.

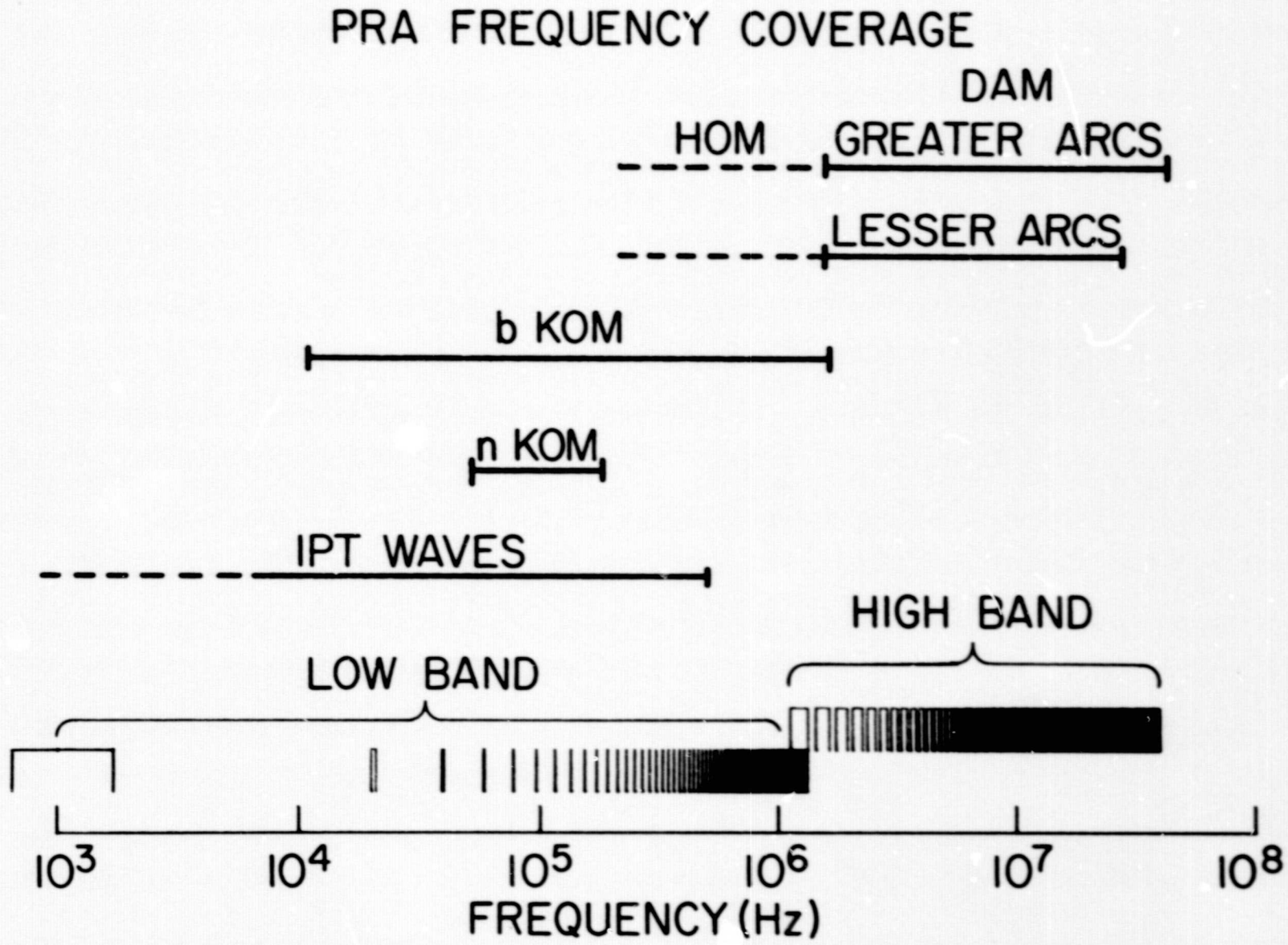
PRA FREQUENCY COVERAGE
DAM
HOM
GREATER ARCS
LESSER ARCS
b KOM
n KOM
IPT WAVES
HIGH BAND
LOW BAND
10^3
10^4
10^5
10^6
10^7
10^8
FREQUENCY (Hz)

Figure 1

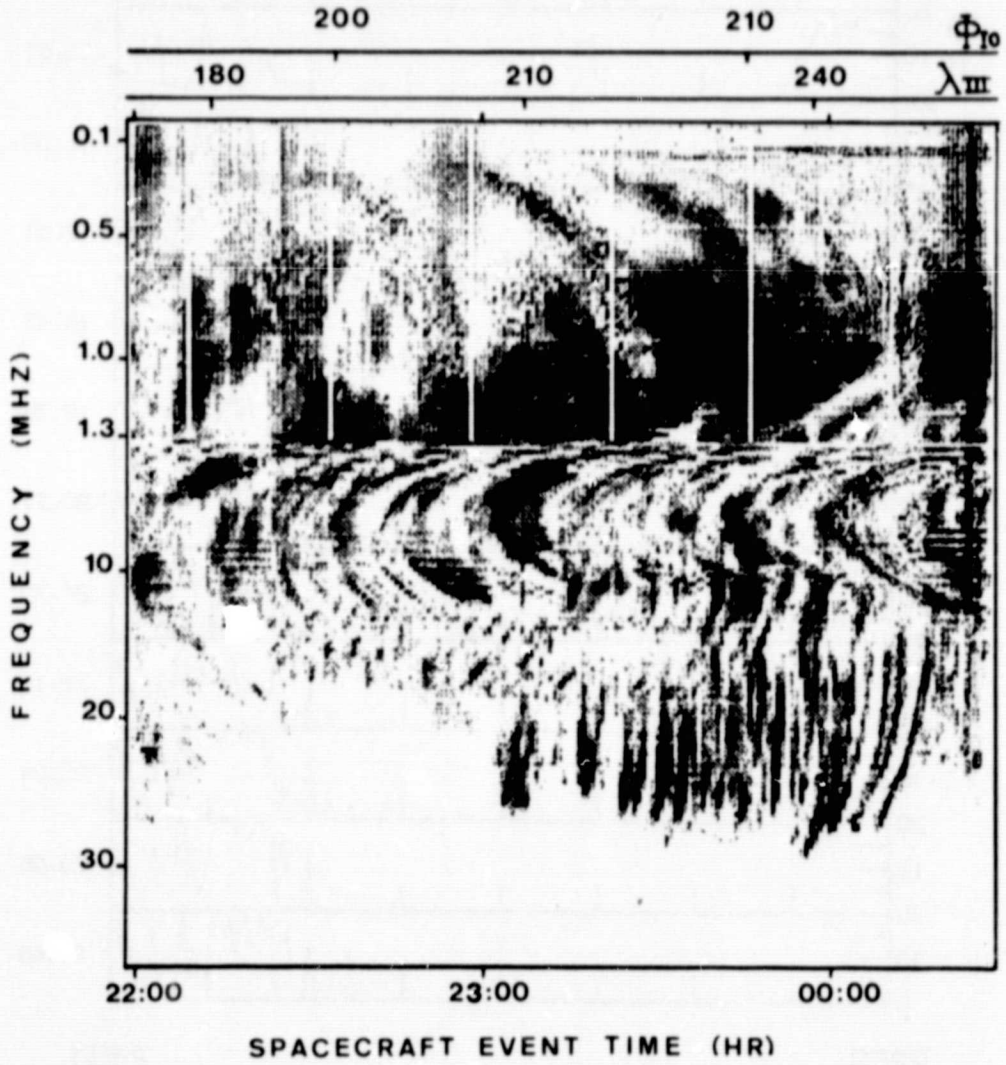
200
210
Φ_{Io}
180
210
240
λ_{III}
0.1
0.5
1.0
1.3
10
20
30
FREQUENCY (MHZ)
22:00
23:00
00:00
SPACECRAFT EVENT TIME (HR)

Figure 2a

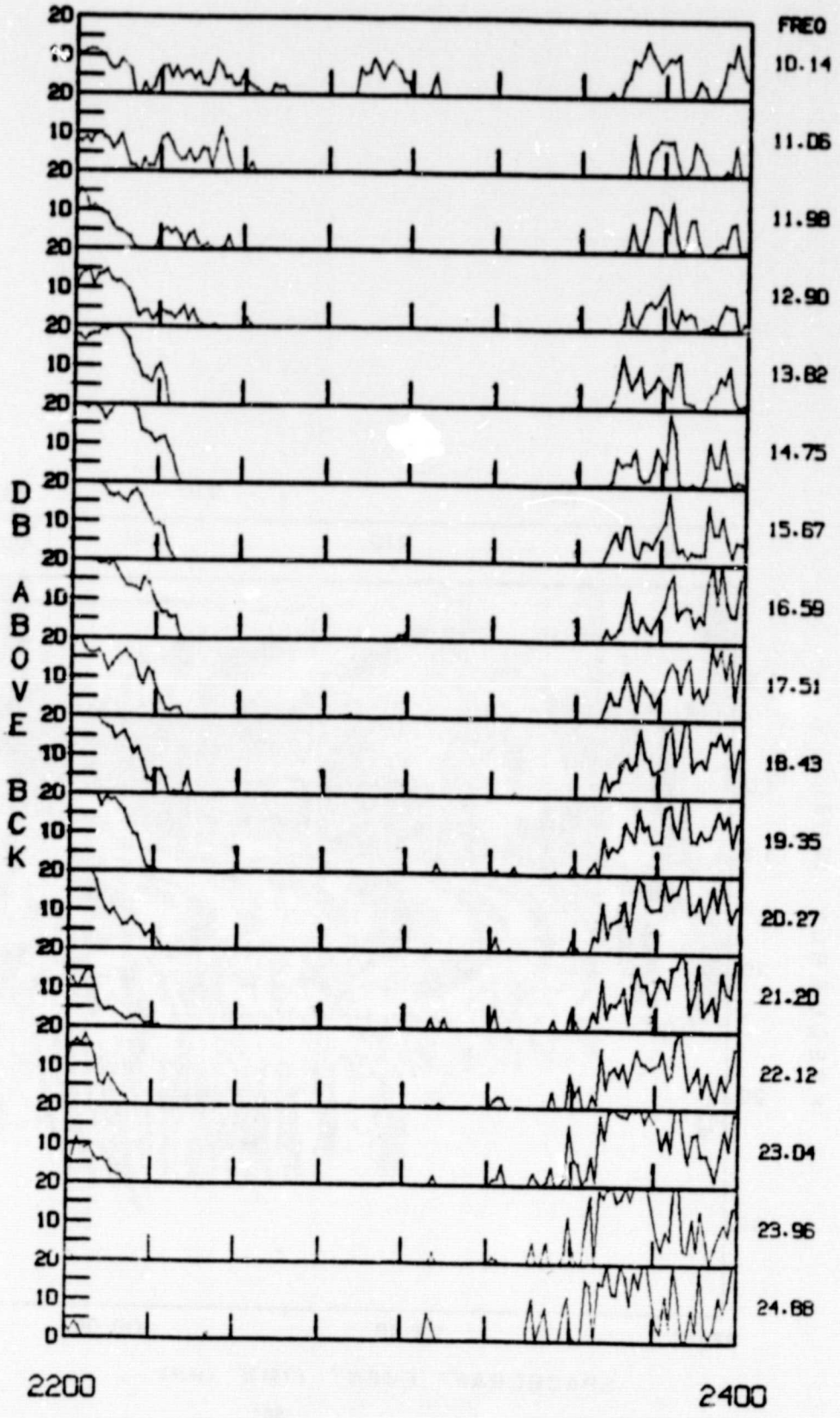

SCET 790305

Figure 2b
(TEMPORARY)

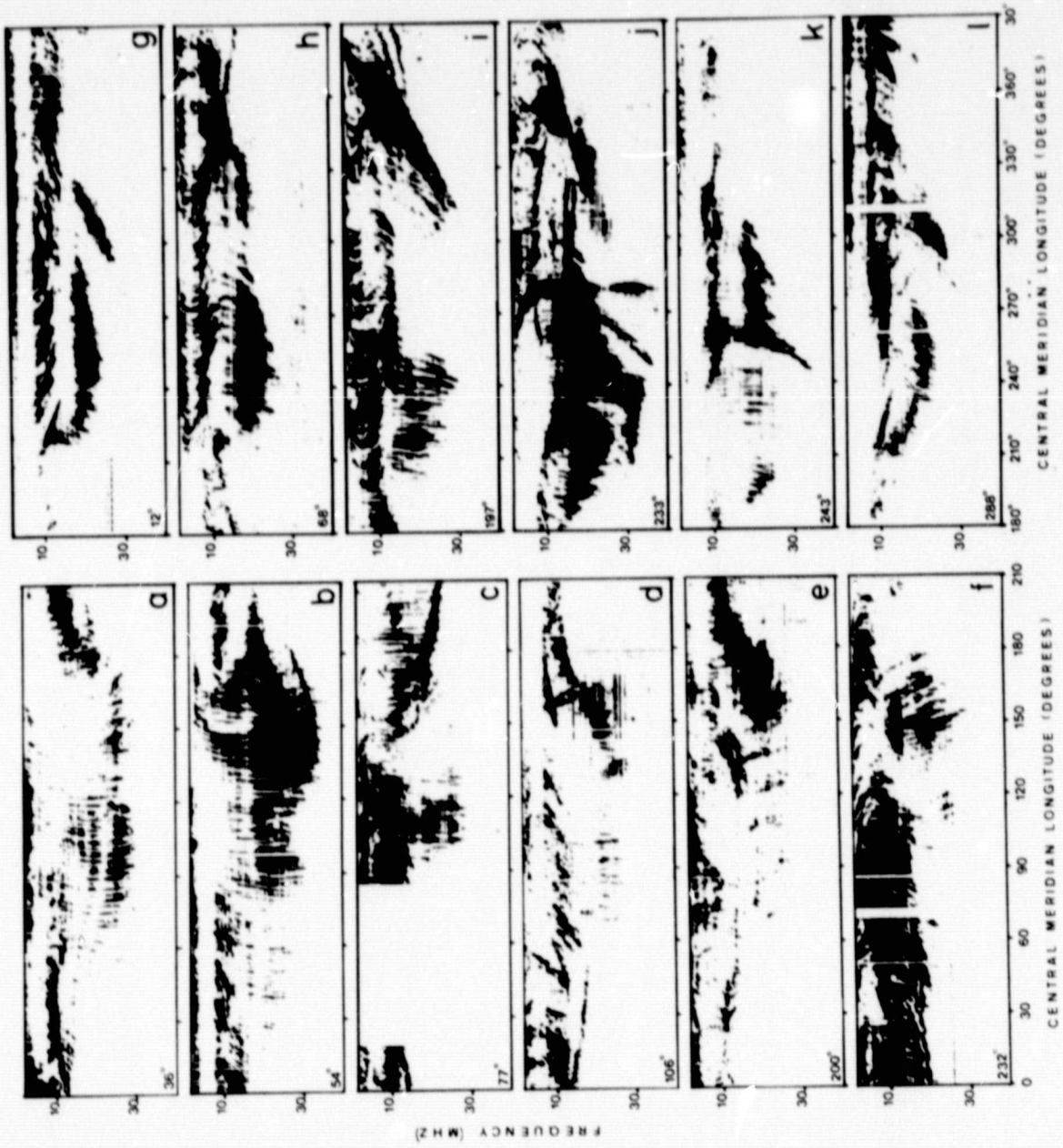
a
b
c
d
e
f
g
h
i
j
k
l
36°
54°
77°
106°
200°
232°
12°
68°
197°
233°
243°
286°
10
30
0
30
60
90
120
150
180
210
180°
210°
240°
270°
300°
330°
360°
FREQUENCY (MHZ)
CENTRAL MERIDIAN LONGITUDE (DEGREES)
CENTRAL MERIDIAN LONGITUDE (DEGREES)

Figure 3

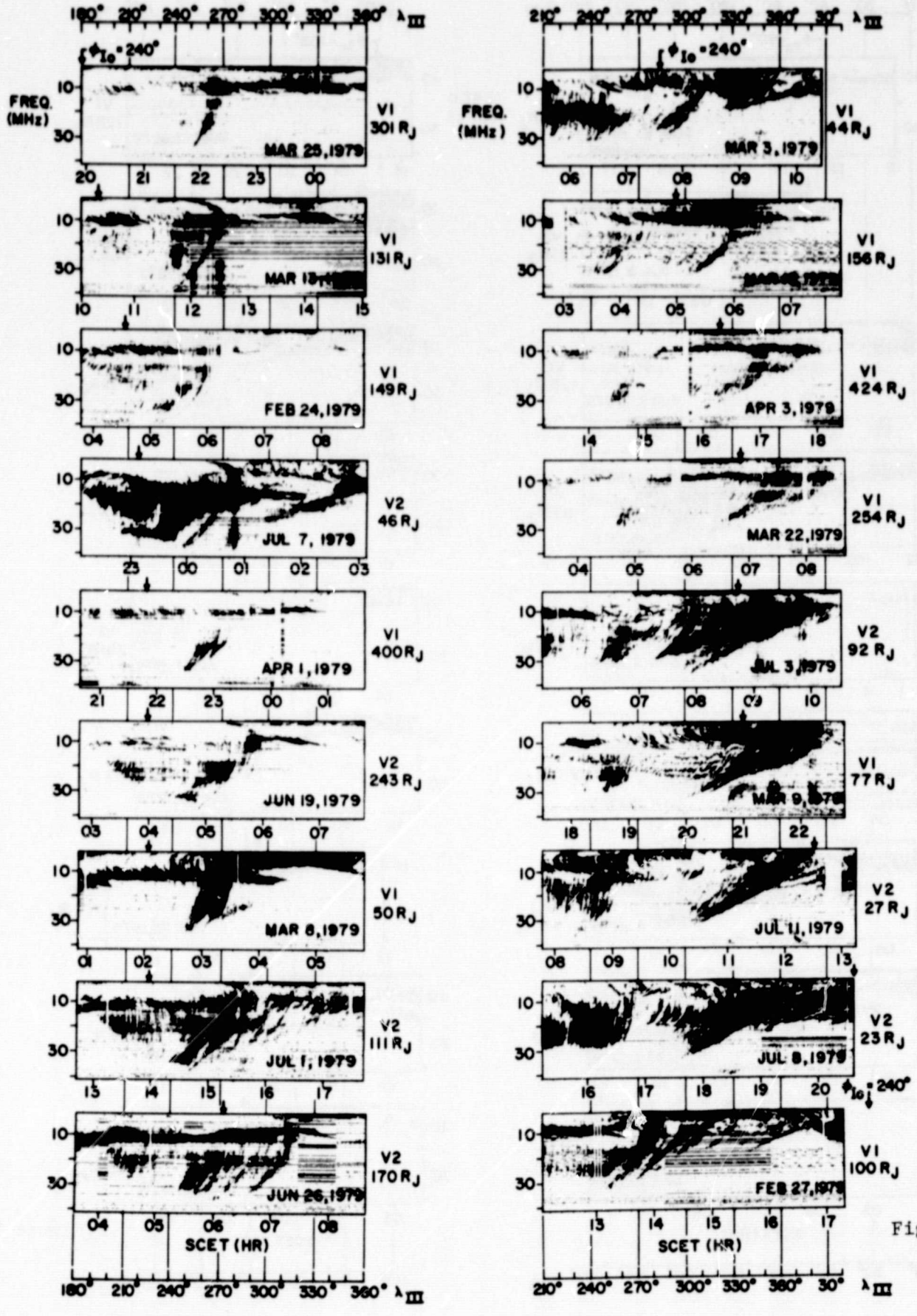

Figure 4a

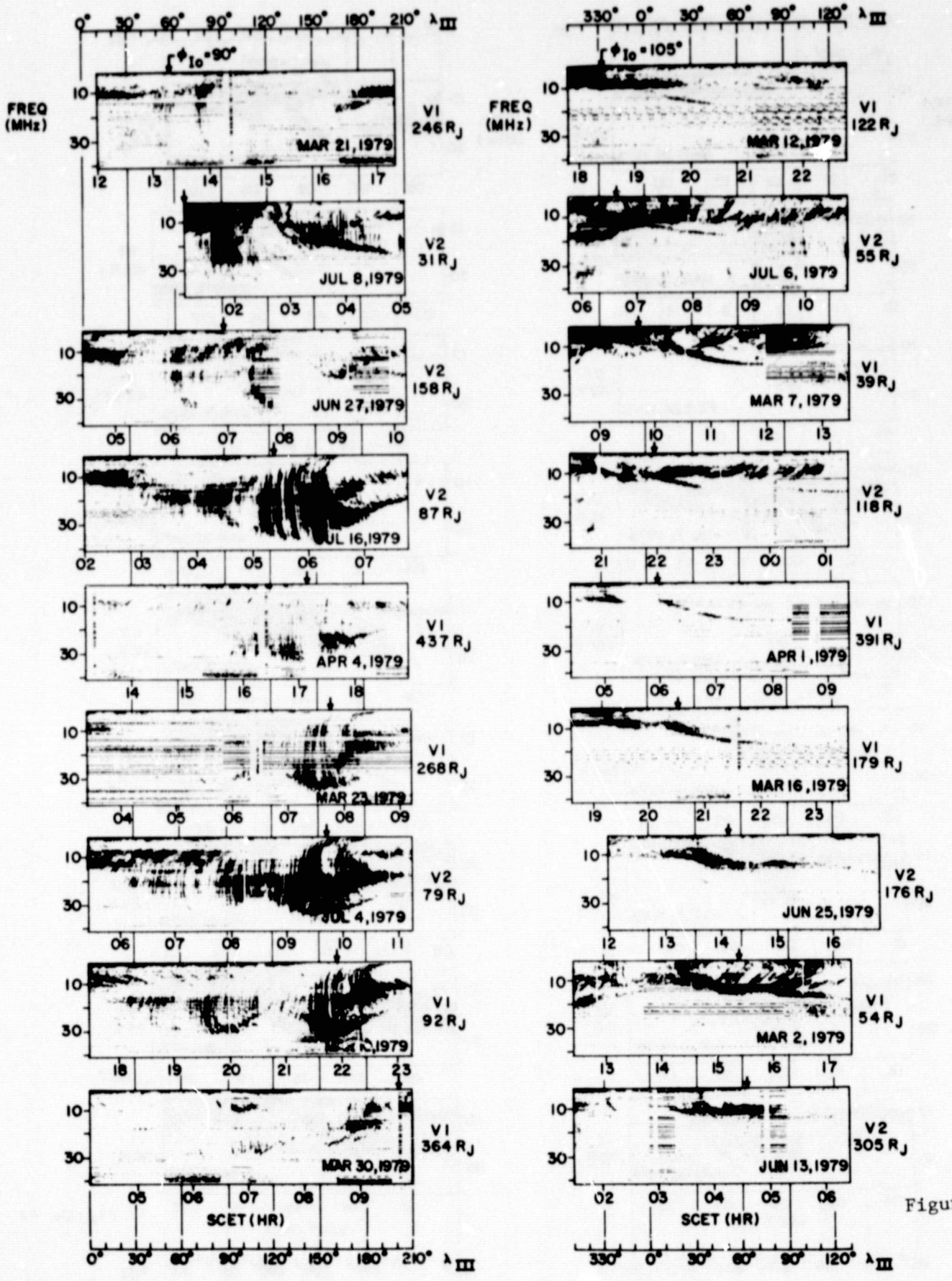
FREQ (MHz)
SCET (HR)
λIII
φIo = 90°
φIo = 105°
MAR 21, 1979
VI 246 RJ
JUL 8, 1979
V2 31 RJ
JUN 27, 1979
V2 158 RJ
JUL 16, 1979
V2 87 RJ
APR 4, 1979
VI 437 RJ
MAR 23, 1979
VI 268 RJ
JUL 4, 1979
V2 79 RJ
MAR 30, 1979
VI 364 RJ
MAR 12, 1979
VI 122 RJ
JUL 6, 1979
V2 55 RJ
MAR 7, 1979
VI 39 RJ
APR 1, 1979
V2 118 RJ
MAR 16, 1979
VI 391 RJ
JUN 25, 1979
V2 179 RJ
MAR 2, 1979
VI 176 RJ
JUN 13, 1979
VI 54 RJ
V2 305 RJ

Figure 4b

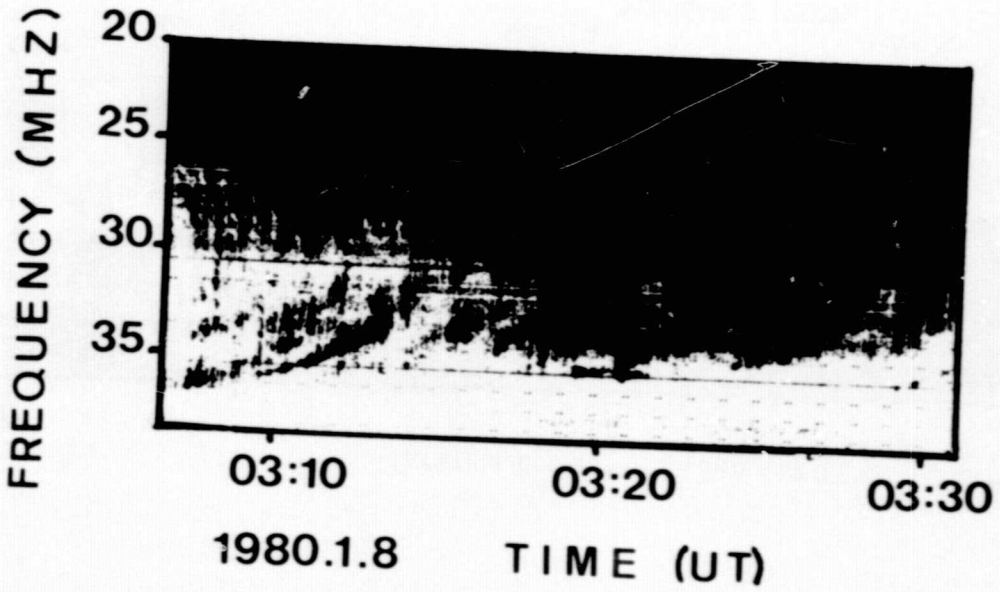

Figure 5

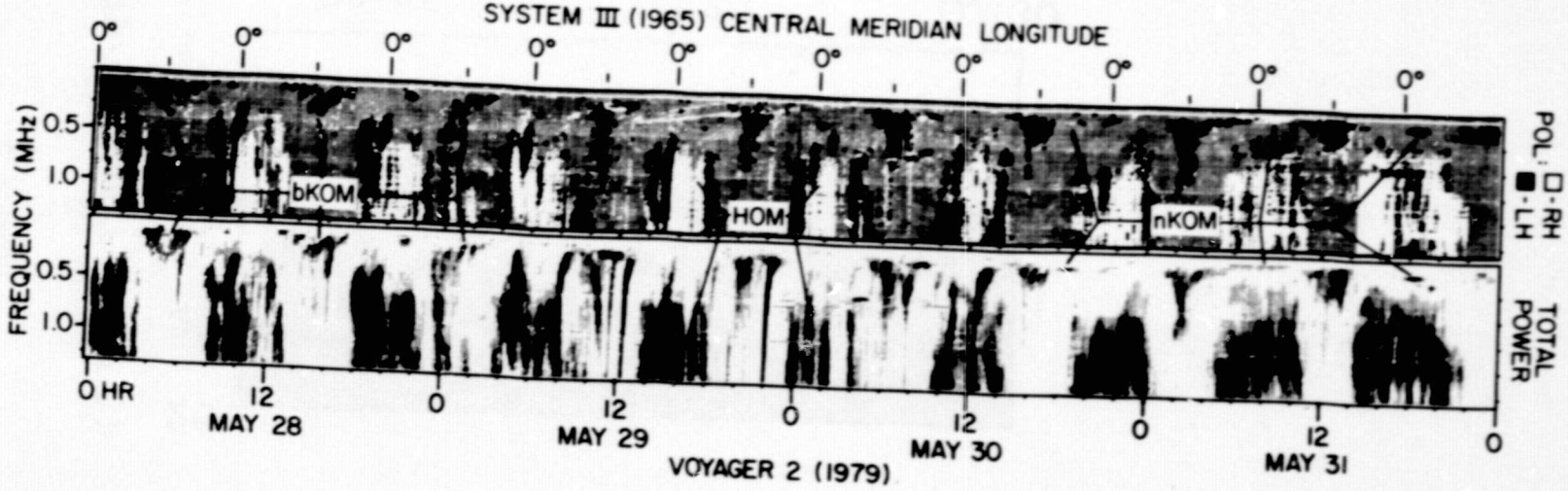
SYSTEM III (1965) CENTRAL MERIDIAN LONGITUDE
0°
FREQUENCY (MHz)
0.5
1.0
bKOM
HOM
nKOM
POL: □-RH ■-LH
TOTAL POWER
0 HR
12
MAY 28
0
12
MAY 29
0
12
MAY 30
0
12
MAY 31
VOYAGER 2 (1979)

Figure 6

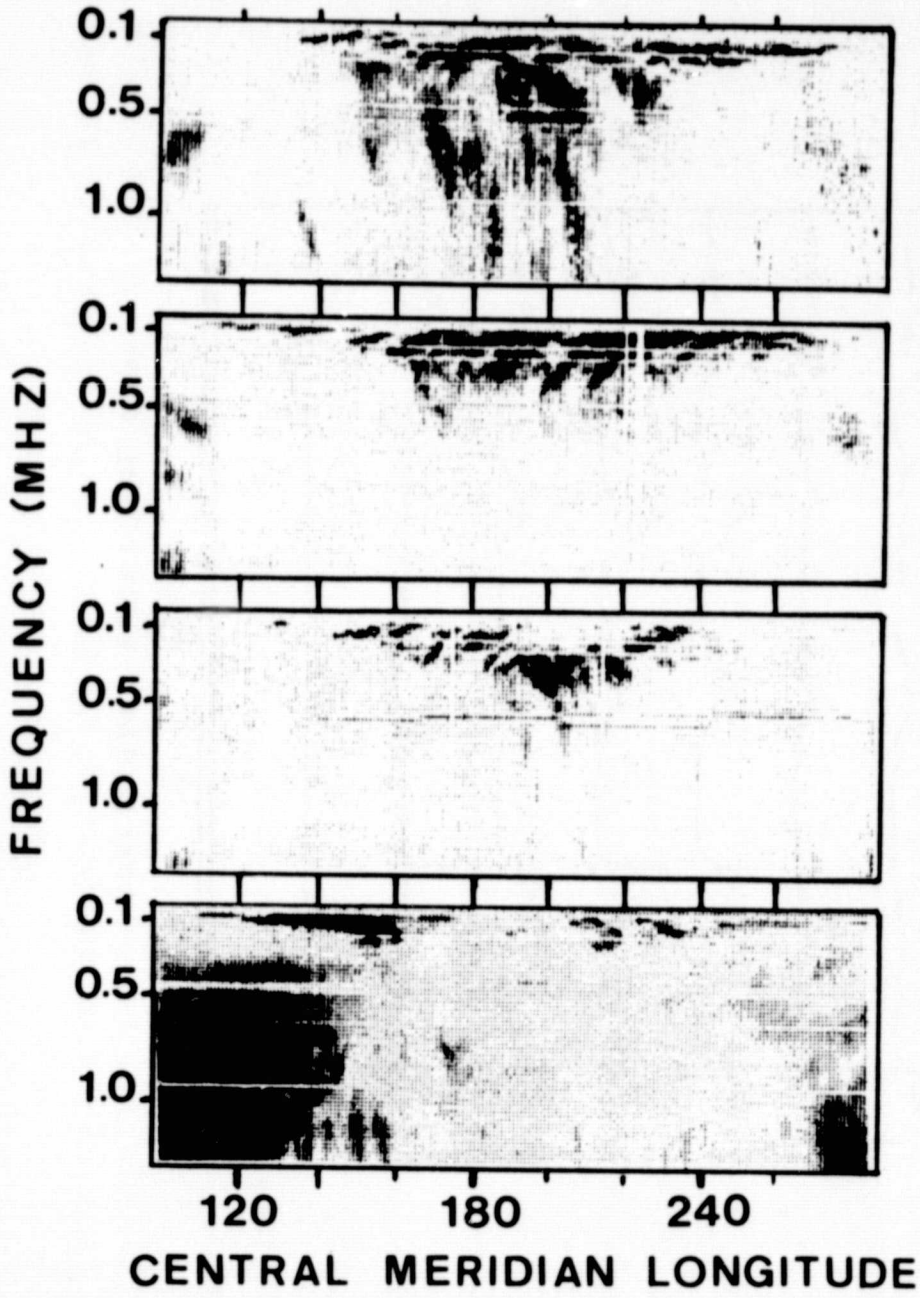

Figure 7

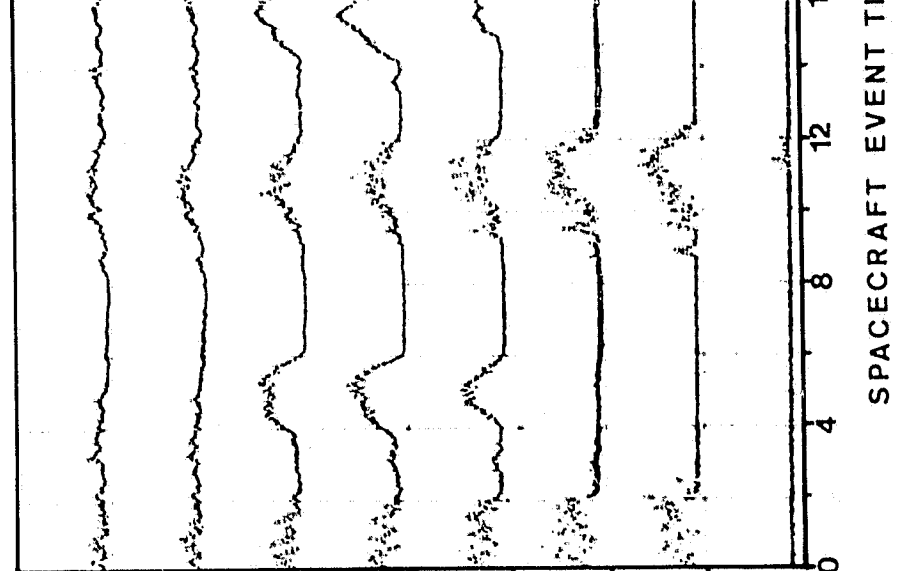
FREQUENCY (KHZ)
10 DB
174
155
116
97
78
59
40
20
0
4
8
12
16
20
SPACECRAFT EVENT TIME (HR)

Figure 8

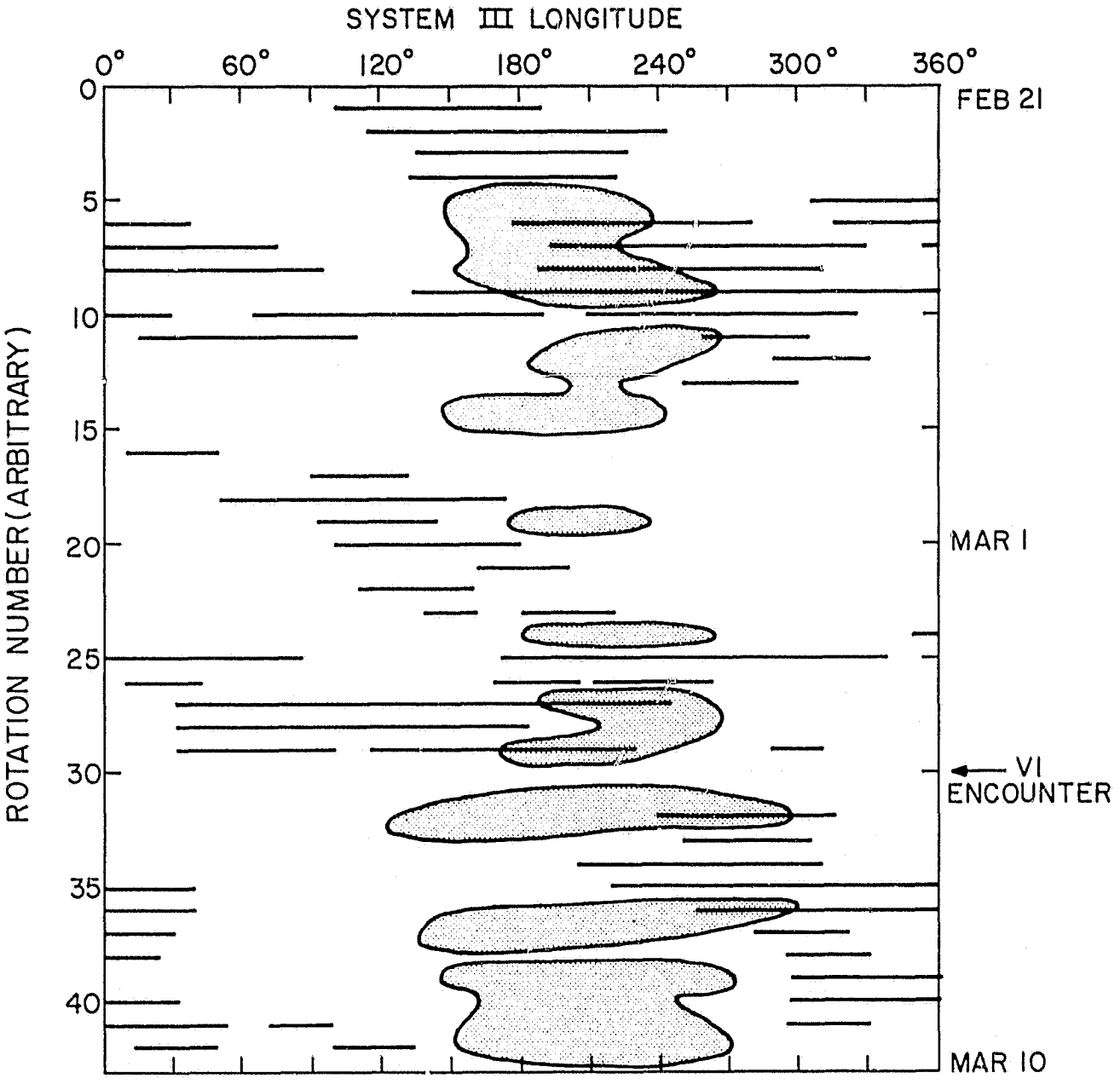
SYSTEM III LONGITUDE
0°
60°
120°
180°
240°
300°
360°
ROTATION NUMBER (ARBITRARY)
0
5
10
15
20
25
30
35
40
FEB 21
MAR 1
VI ENCOUNTER
MAR 10

Figure 9a

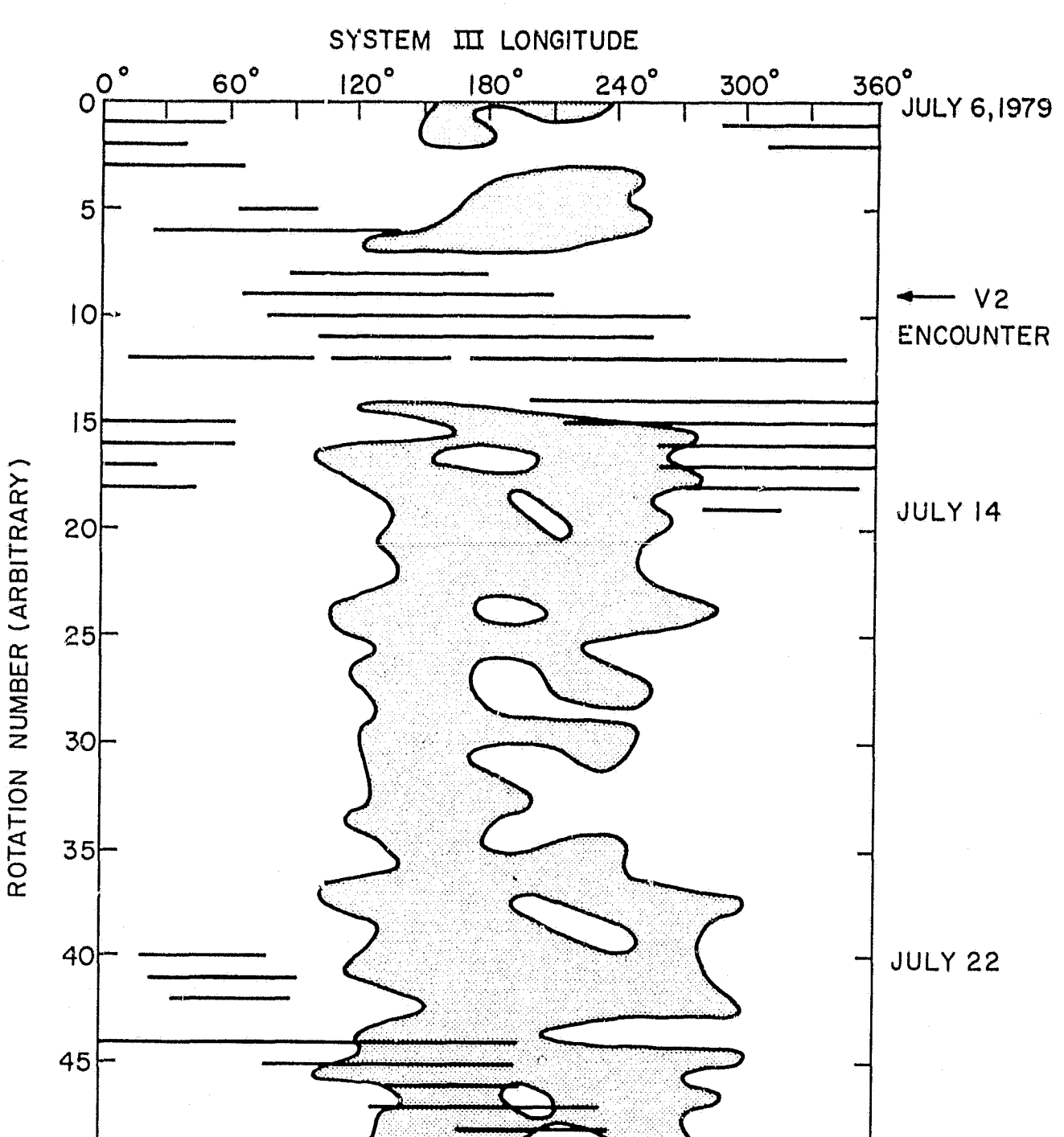
SYSTEM III LONGITUDE
0°
60°
120°
180°
240°
300°
360°
0
5
10
15
20
25
30
35
40
45
50
ROTATION NUMBER (ARBITRARY)
JULY 6, 1979
V2 ENCOUNTER
JULY 14
JULY 22
JULY 27

Figure 9b

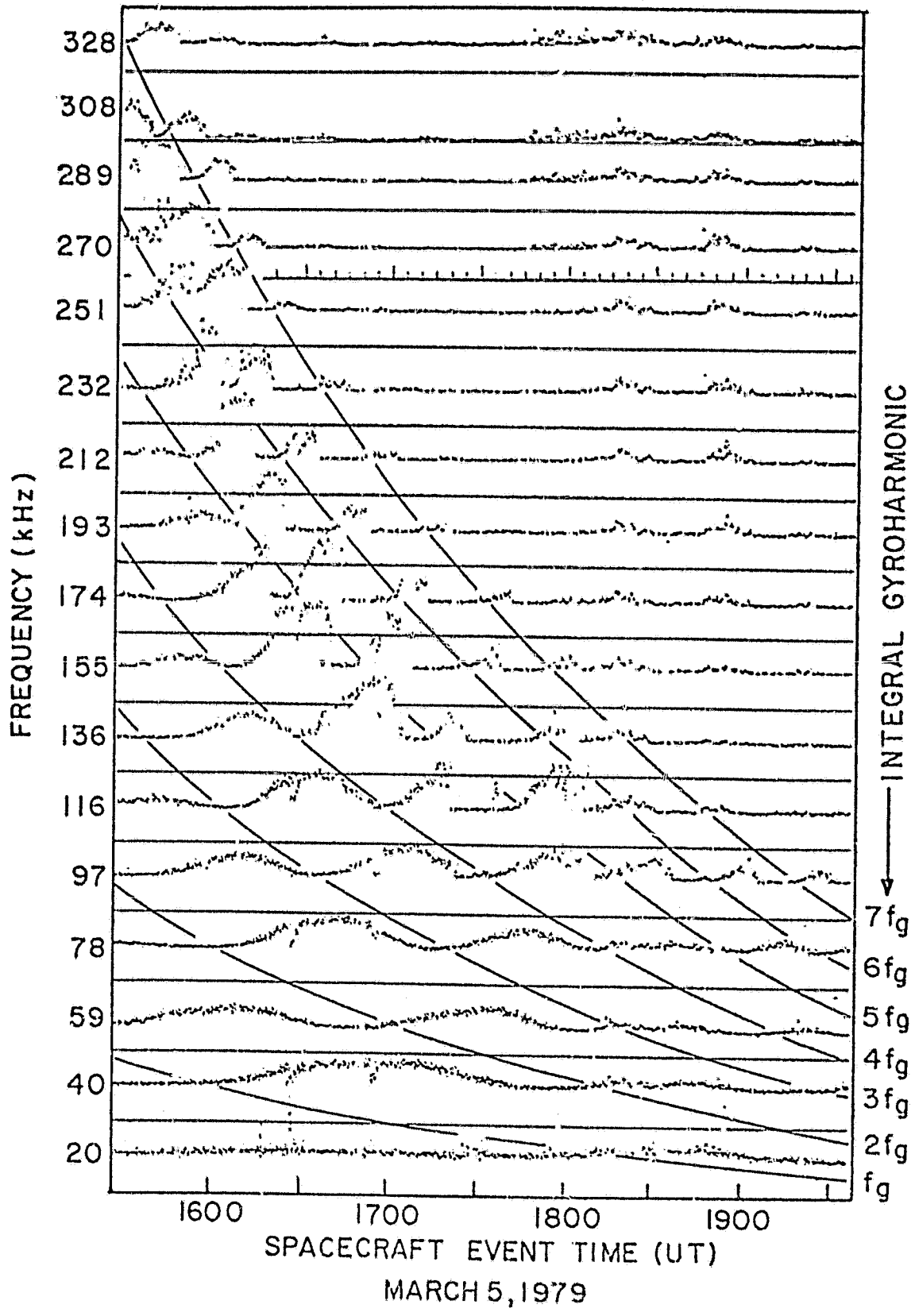
328
308
289
270
251
232
212
193
174
155
136
116
97
78
59
40
20
FREQUENCY (kHz)
INTEGRAL GYROHARMONIC
7fg
6fg
5fg
4fg
3fg
2fg
fg
1600
1700
1800
1900
SPACECRAFT EVENT TIME (UT)
MARCH 5, 1979

Figure 10